Received: 30 August 2019 | Revised: 14 September 2019 | Accepted: 16 September 2019

DOI: 10.1002/inf2.12050

ORIGINAL ARTICLE

WILEY

Spatial variations of valley splitting in monolayer transition metal dichalcogenide

Chenji Zou[1] | Hongbo Zhang[1] | Yu Chen[1] | Shun Feng[1] | Lishu Wu[1] | Jing Zhang[1] | Ting Yu[1] | Jingzhi Shang[2] | Chunxiao Cong[3]

[1]Division of Physics and Applied Physics, School of Physical and Mathematical Sciences, Nanyang Technological University, Singapore, Singapore

[2]Institute of Flexible Electronics, Northwestern Polytechnical University, Xi'an, Shaanxi, China

[3]State Key Laboratory of ASIC and System, School of Information Science and Technology, Fudan University, Shanghai, China

Correspondence

Ting Yu, Division of Physics and Applied Physics, School of Physical and Mathematical Sciences, Nanyang Technological University, 21 Nanyang Link, Singapore 637371, Singapore.
Email: yuting@ntu.edu.sg

Chunxiao Cong, State Key Laboratory of ASIC and System, School of Information Science and Technology, Fudan University, Shanghai 200433, China.
Email: cxcong@fudan.edu.cn

Funding information

National Natural Science Foundation of China, Grant/Award Numbers: 61774040, 11774170; Singapore Ministry of Education (MOE) Tier 1, Grant/Award Number: RG199/17; The Fudan University-CIOMP Joint Fund, Grant/Award Number: FC2018-002; The National Key R&D Program of China, Grant/Award Number: 2018YFA0703700; The National Young 1000 Talent Plan of China; The Shanghai Municipal Natural Science Foundation, Grant/Award Number: 16ZR1402500; The Shanghai Municipal Science and Technology Commission, Grant/Award Number: 18JC1410300

Abstract

In monolayer group-VI transition metal dichalcogenides (TMDs), valley splitting features have received a lot of attention since it can be potentially utilized for information storing and processing. Among the known two-dimensional (2D) TMDs, monolayer WSe_2 or $MoSe_2$ has been mostly selected for excitonic and valleytronic physics studies because of its sharp and well-resolved excitonic spectral features. Meanwhile, their high optical quality leads to a tremendous desire for developing promising WSe_2- and $MoSe_2$-based valleytronic devices. Toward this goal, exploring the uniformity of valley features crossing an entire piece of monolayer becomes necessary and critical. Here, we performed the systematic magneto-photoluminescence mapping measurements on mechanically exfoliated monolayer WSe_2 and observed unconventional spatial variations of valley splitting. The observed nonuniformity is attributed to the modulated doping, which is probably due to the different distributions of unintentional absorbates across the sample. Such an unexpected doping effect shows the nonnegligible influence on the valley Zeeman splitting of the trion emission (X_T) while affecting that of the neutral exciton emission (X_0) trivially, evidencing for the large valleytronic sensitivity of the charged exciton. This work not only enriches the understanding of the doping effect on valley splitting but also is meaningful for developing 2D valleytronics.

KEYWORDS

doping effect, monolayer WSe_2, photoluminescence, transition metal dichalcogenide, valley splitting

1 | INTRODUCTION

Monolayer (ML) transition metal dichalcogenides (TMDs) in the class of MX_2 (M = Mo, W; X = S, Se) are one branch of two-dimensional (2D) materials that attract numerous attention due to their direct-bandgap structures, overcoming the shortages of the gapless in graphene.[1-10] Moreover, the broad families of TMDs cover the whole visible frequency range and become promising candidates for the next-generation electronics and optoelectronics.[11-14] Besides the direct-bandgap nature of ML MX_2, the inversion symmetry breaking of ML MX_2 leads to a large spin-orbit coupling (SOC),[15-17] which further results in the splitting of valance bands at K and K' valleys. This splitting of valance bands can be probed as A and B excitons through circularly polarized optical methods. In addition to the strong SOC in ML TMDs, K and K' valleys are energy-degenerated but inequivalent due to the time-reversal symmetry.[18,19] This energy degeneracy can be lifted upon an out-of-plane external magnetic field due to the time-reversal symmetry breaking.[20-25] Among these MX_2, ML WSe_2, and $MoSe_2$ provide a good platform to study the valley splitting phenomena due to their well-resolved excitonic features at low temperatures.[20-23] The high optical quality of ML WSe_2 and $MoSe_2$ also makes them promising for 2D valleytronics devices. Hence, investigation of the uniformity of valley features crossing an entire piece of ML is crucial. Although there are some works studying the doping influence on the valley splitting by applying electric field,[23,26,27] studies of valley splitting variations crossing the ML TMDs are still rare.

In this work, the valley splitting variations crossing the WSe_2 ML are studied by circularly polarized magneto-photoluminescence (PL) mapping. With the spatial evolution crossing the samples, there is a gradual doping effect that can be manifested by the blueshifts of trion (X_T) and A exciton (X_0) emissions. The different doping regions indicate the different electron-electron interaction strength, which further influences the valley splitting behaviors of the ML WSe_2. Particularly, the valley splitting behavior of X_0 emission is almost independent of the doping level while the doping level plays a critical role in the valley splitting behavior of X_T emission. The size-dependent doping is found to be relevant with the variation of the valley splitting behavior.

By using the all-dry-transfer method, the WSe_2 flake was transferred onto the 300 nm SiO_2/Si substrate. Figure 1A shows the optical image of the exfoliated WSe_2 flake and the white arrow represents the spatial evolution path discussed later. The absence of the dominant Raman peak E_{2g} around 250 cm^{-1} and the frequency of A_{1g} mode suggest that our sample is ML WSe_2 (see Figure 1B).[28,29] To trace the spatial evolution of PL spectra, a contour plot of peak position crossing the exfoliated ML WSe_2 is given at both 77 and 4.2 K (see Figure 1C,D), where the center position is defined as 0 μm. As shown in the contour mapping, both X_T and X_0 emissions show the blueshifts as the spatial location changes from the center to the edge (indicated by the white dashed line in Figure 1A). PL spectra are extracted from the center and edge regions at both 77 and 4.2 K (see Figure 1E, F). The well-resolved trion and exciton emissions present in the PL spectra at both 77 and 4.2 K. At 4.2 K, the X_0 and X_T emissions locate at ~1.74 and ~1.71 eV respectively[20,22,30,31]; meanwhile, two localized-state emissions labeled as L_1 and L_2 are observed. According to previous studies, the exfoliated WSe_2 often shows a P-type doping and thus the trion emission is positively charged. At the edge region of the ML WSe_2, the PL spectrum is shown in the lower panel of Figure 1F, where one more localized-state emission labeled as L_3 appears. The presence of these localized emissions at 4.2 K is associated with the greater suppression of thermal fluctuation compared to that at 77 K.[32,33] Moreover, the increase of intensity ratio between the X_T and X_0 emissions at the edge region suggests that more holes are localized at the edge region, which facilitate the formation of more positive trions. Theoretical calculations have shown that the atmosphere O_2 and H_2O can be physically absorbed on the surface of TMDs and even more tightly absorbed at the defective sites with a higher charge transfer, where the hole doping is expected for the physical absorption of O_2 and H_2O onto 1 L WSe_2.[34] As a consequence, the high P-type doping is expected around the more defective sample edge than the one near the center region, which supports our observations here. To visualize the peak evolution quantitatively, single spectra are extracted from PL mapping data with the scanning step of 400 nm. The peak positions of X_T and X_0 emissions are plotted along the spatial locations (see Figure S1). From Figure S1c, a blueshift of ~5 meV is obtained for X_T emission between the center and the edge regions at 4.2 K. While for X_0 emission (see Figure S1d), this blueshift is ~8 meV. The blueshifts of X_T and X_0 emissions can be understood as follows. Quantitatively, the X_0 energy is determined by the equation $E_{exc} = E_g - E_b$, where E_g is the electronic bandgap, which is defined by the total energies needed to separately tunnel an electron and a hole and the X_0 energy of E_{exc} is also known as the optical bandgap; E_b is the X_0 binding energy, which is usually probed by PL spectra compared with the electronic bandgap of E_g.[35] In 2D materials, many-body interactions due to quantum confinement are enhanced compared with the ones of the 3D systems since they are almost compensated by the attractive long-range correlations.[36] When scaling down to 2D materials, the long-range Coulomb correlation is less efficient and the short-range exchange (eg, electron-electron interaction) having its origin in the Pauli exclusion principle becomes dominant.[37] This short-range

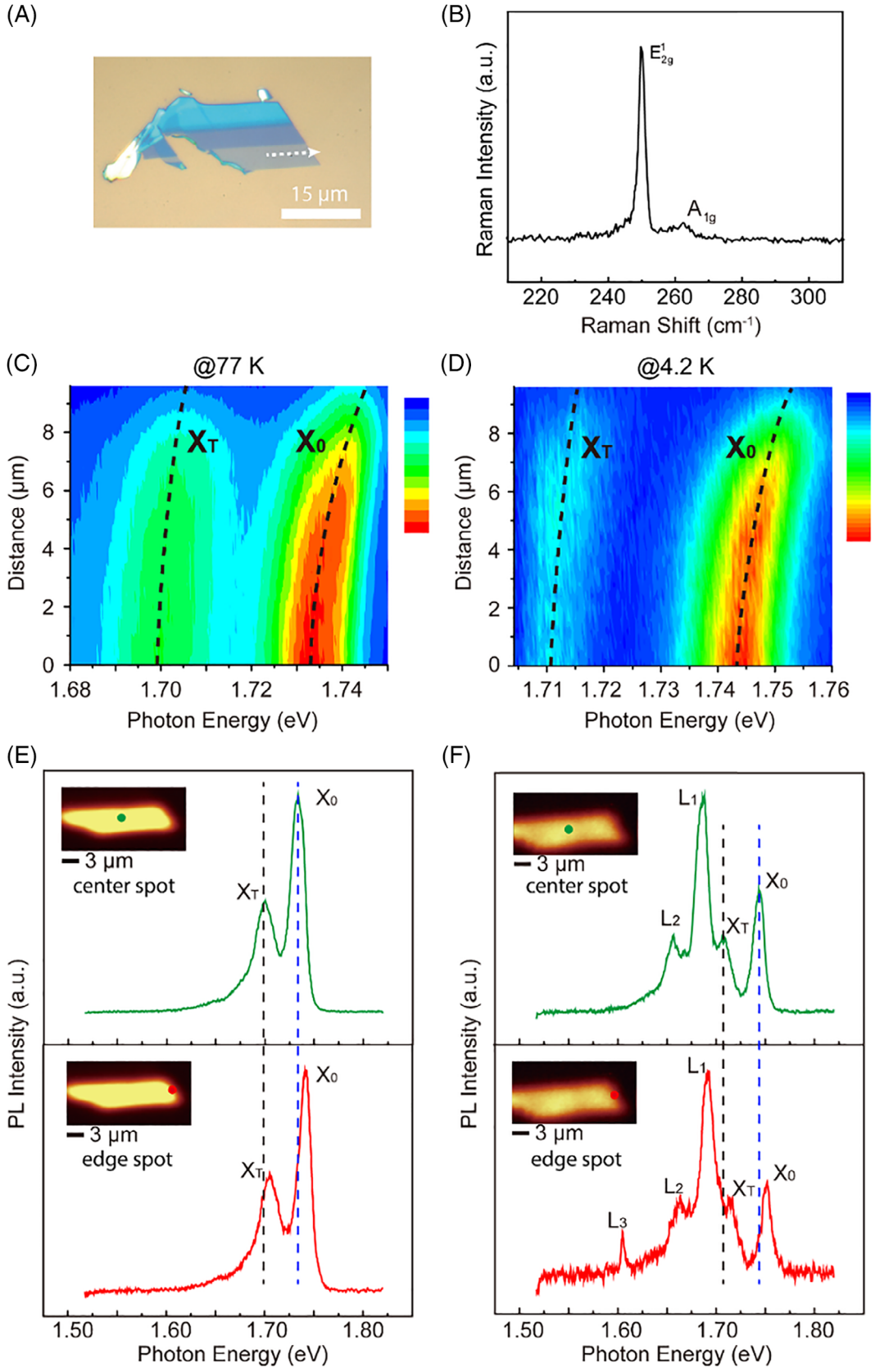

FIGURE 1 A, Optical images of exfoliated WSe_2, the white dashed arrow indicates the direction of spatial evolution from the center to the edge. B, Raman spectrum of presented WSe_2 flake @RT. C, Contour plot of peak position crossing the exfoliated WSe_2 (define the center as 0 μm) @ 77 K. D, Contour plot of peak position crossing the exfoliated WSe_2 (define the center as 0 μm) @ 4.2 K. E, PL spectra @77 K acquired from the center and edge regions indicated by green and red spots in the PL mapping inset (extracted by the integrated intensity from 1.54 to 1.77 eV). F, PL spectra @4.2 K acquired from the center and edge regions indicated by green and red spots in the PL mapping inset (extracted by the integrated intensity from 1.54 to 1.77 eV)

exchange of electron gas further affects the X_0 energy as shown in Figure S2: there is a reduction of electronic bandgap E_g due to Pauli blocking. Meanwhile, the screening induced by short-range exchange effects decreases the binding energy of the X_0.[38] Thus, the total changing of X_0 energy is a result of these two factors.

Beyond the evolution of PL peaks along spatial locations, valley splitting behaviors of X_T and X_0 emissions are also studied at the center and the edge of the exfoliated WSe_2. The schematic of our circularly polarized PL measurement setup is illustrated in Figure 2A. A polarizer and a quarter-wave plate are used to generate either the σ^+ or the σ^- circularly polarized excitation. Above the beam splitter, another polarizer is used to selectively acquire the σ^+ or the σ^- signals. The excitation laser wavelength is 532 nm (2.33 eV). As clearly shown in Figure 2B,C, the sample nonuniformity is visualized across all the magnetic fields. At edge area, there are clear blueshifts for both X_T and X_0 emissions compared with the ones from the center area. Without the magnetic field ($B = 0$ T), there are no differences between σ^+/σ^+ and σ^-/σ^- for both X_T and X_0 emissions. In Figure 2B, upon an external magnetic field, the X_T peak position under σ^+/σ^+ and σ^-/σ^- shifts oppositely with each other compared with that at zero field. Similar phenomenon can also be observed for X_0 emission in Figure 2C. More detailed PL images of the X_T and X_0 emission energies under different magnetic fields under σ^+/σ^+ and σ^-/σ^- configurations are provided in Figure S3.

To more intuitively clarify valley splitting behaviors of X_T and X_0 emissions, typical polarization-resolved PL spectra extracted from the center and edge regions with σ^+/σ^+ and σ^-/σ^- configurations at selected magnetic fields are given in Figure 3. The extracted splitting energies that are the statistical average values of both X_T and X_0 emissions at selected center and edge areas (marked in Figure 2C) are given in Figure 4. At the center area, the valley splitting energies of X_T emission show a linear relationship with the external magnetic field and the slope is -0.231 ± 0.011 meV/T (see green fitting in Figure 4A). For X_0 emission, the valley splitting energies also show a linear dependence with the external magnetic field and the slope is -0.237 ± 0.005 meV/T (see green fitting in Figure 4B). The slope for the X_T emission corresponds closely to that of the X_0 emission, which is consistent with previous literature.[21,23,39] At the edge area, the valley splitting dependence of X_T emission on the magnetic field becomes nonlinear, which is different from the linear case at the center region (see red curve in Figure 4A), which is attributed to the impact of strong Coulomb interactions on valley magnetic response of charged excitons.[26] While for the X_0 emission, the valley splitting energies still show a linear dependence with the external magnetic field (see green fitting in Figure 4B) and the slope is -0.239 ± 0.003 meV/T. Moreover, the slope for the X_0 emission at the edge region corresponds closely to that of at the center region. This reveals that the valley splitting

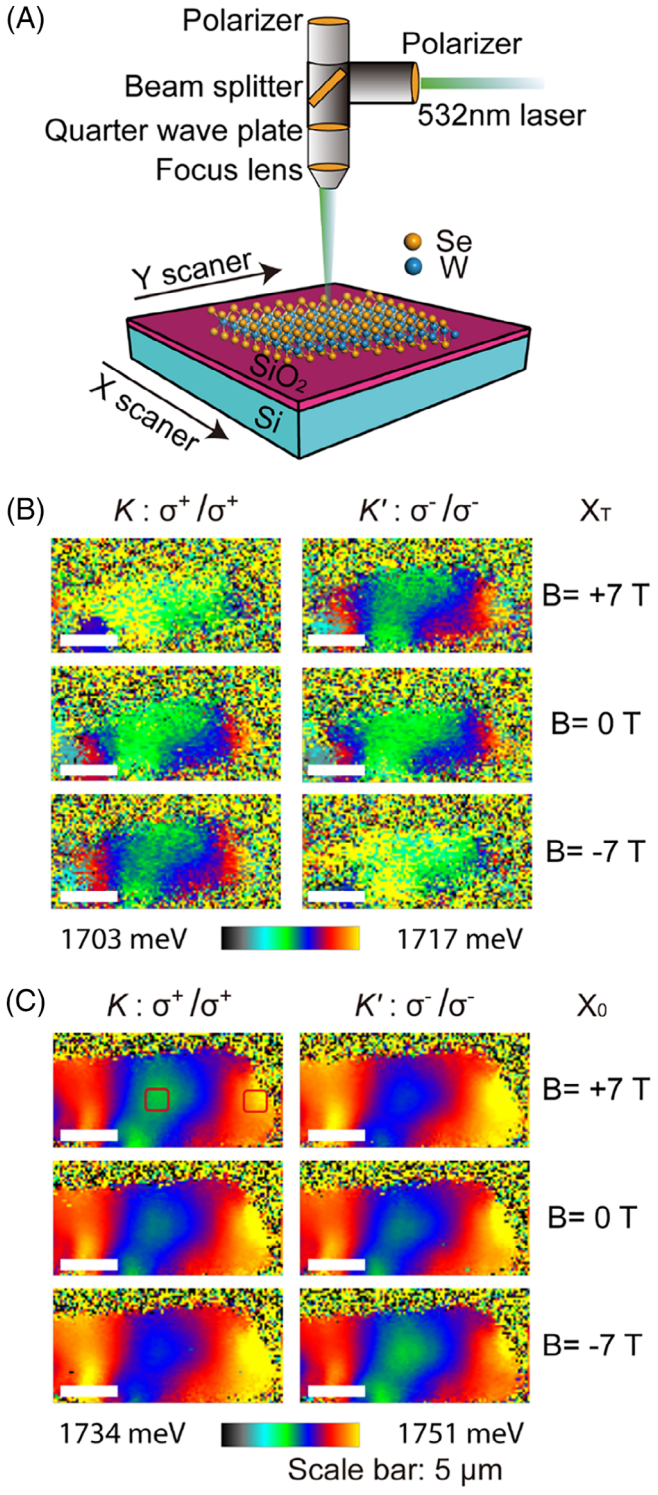

FIGURE 2 A, A detailed schematic of the circularly polarized PL measurement setup. B, PL images of X_T emission energies under the magnetic fields of 7, 0, and −7 T with σ^+ and σ^- polarizations. C, PL images of the X_0 emission energies under the magnetic fields of 7, 0, and −7 T with σ^+ and σ^- polarizations

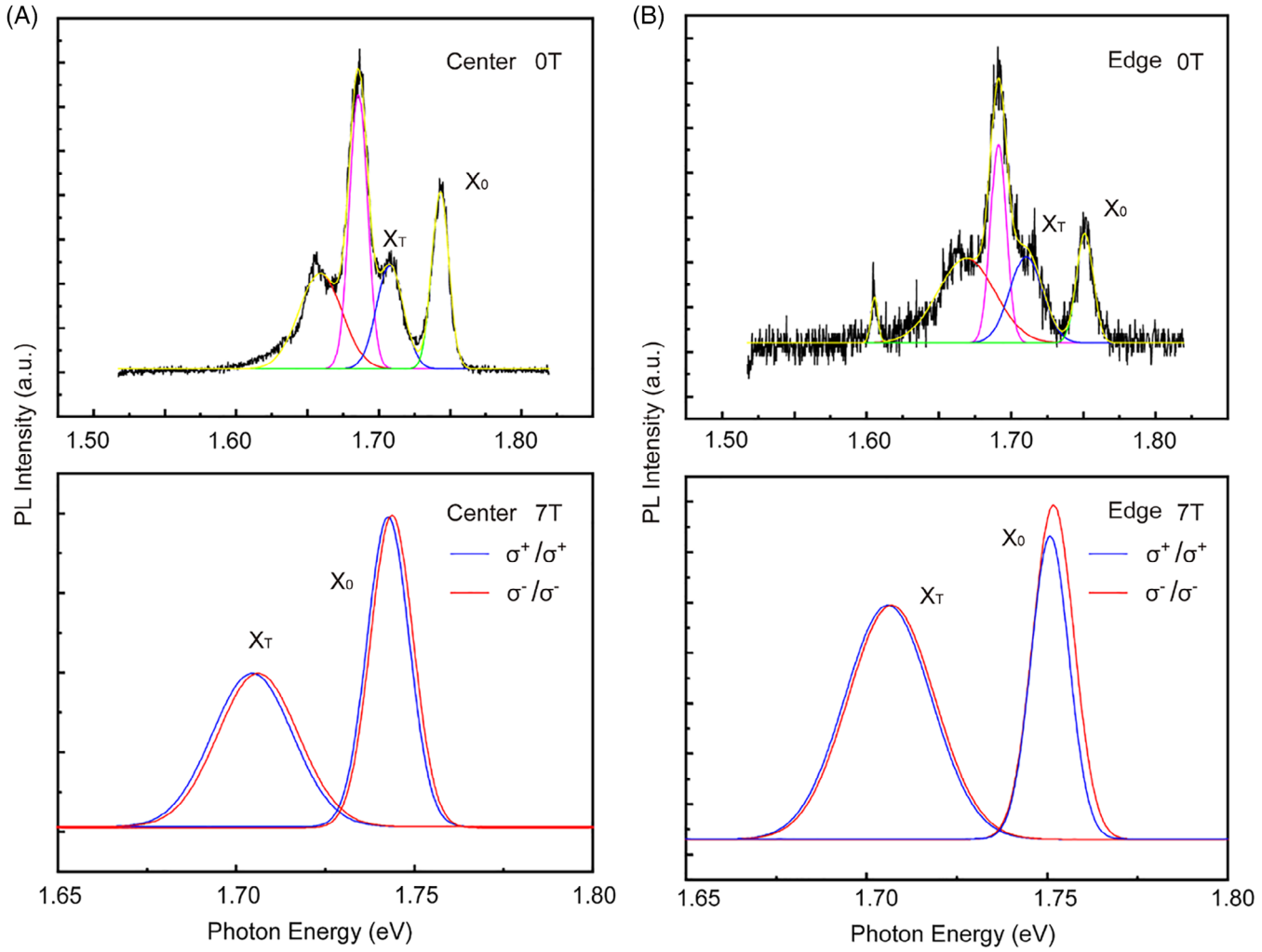

FIGURE 3 A, PL spectra of monolayer WSe_2 extracted from the center area under 0 T and under 7 T with σ^+ and σ^- polarizations. B, PL spectra of monolayer WSe_2 extracted from the edge area under 0 T and under 7 T with σ^+ and σ^- polarizations

behavior of X_0 emission is nearly independent of the doping density.

Similar experiments were conducted on a smaller ML WSe_2 flake. A contour plot of the peak position crossing the smaller exfoliated WSe_2 is given at 77 K (see Figure S4a). Unlike the obvious shifts of X_T and X_0 emissions on the larger ML WSe_2 discussed above, there are much smaller shifts of X_T and X_0 emissions for the smaller flake. The smaller energy shifts of X_T and X_0 emissions imply that the doping levels between the center and edge regions of the smaller flake have a smaller difference compared to that of the larger flake. The smaller energy shifts can be more intuitively observed from Figure S4b. The valley splitting between $\sigma^+/\ \sigma^+$ and σ^-/σ^- configurations at the selected magnetic fields for the center and the edge area are given in Figure S5. For the X_0 emission, the valley splitting energies extracted from the center and the edge areas are nearly identical, which is consistent with the previous discussion. A more detailed valley splitting energies of X_T and X_0 emissions as a function of external magnetic field from the center and the edge area are given in Figure S6. At the center area, the valley splitting energies of X_T emission show a linear relationship with the external magnetic field and the slope is -0.230 ± 0.005 meV/T (see green fitting in Figure S6a). While for X_0 emission, the valley splitting energies also show a linear dependence with the external magnetic field and the slope is -0.232 ± 0.001 meV/T (see green fitting in Figure S6b). Both slopes of X_T and X_0 emissions give a g-factor around 4, which implies the nearly neutral states at the center area. At the edge area, the valley splitting energies of X_T emission still exhibit a linear relationship with the magnetic field and the slope is -0.200 ± 0.006 meV/T (see red fitting in Figure S6a), which is smaller compared to that extracted from the center area. The slope for the X_0 emission at the edge region (-0.231 ± 0.004 meV/T, see red fitting in Figure S6b) corresponds closely to that of at the center region, which

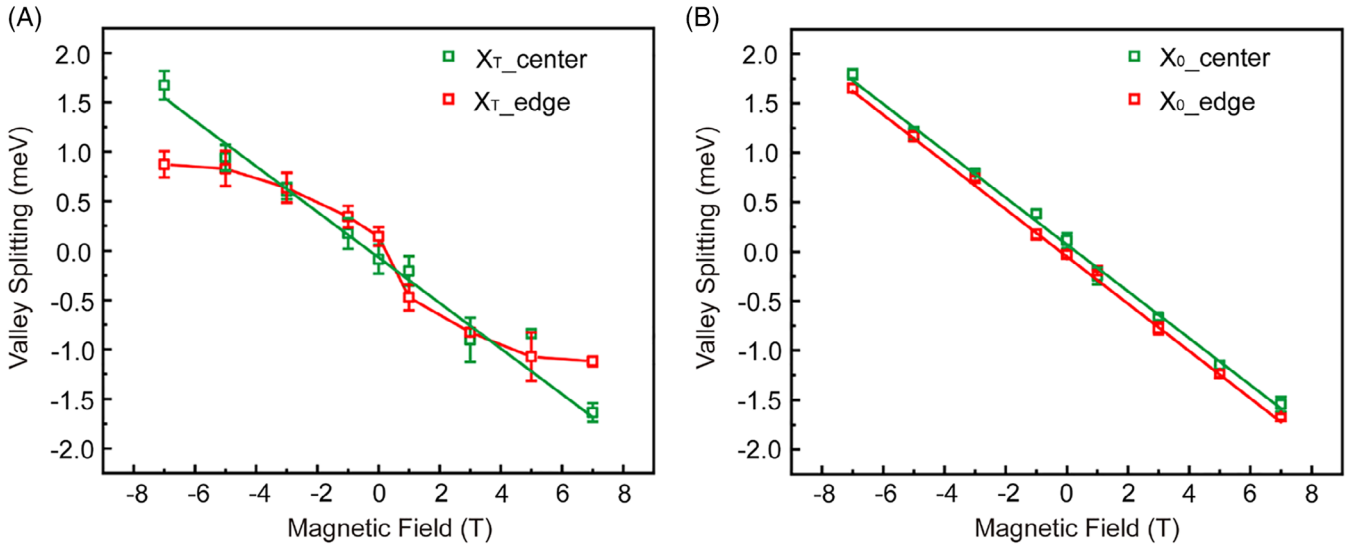

FIGURE 4 A, Valley splitting energies of X_T emission as a function of the magnetic field, the green data points are collected from the center area and the red data points are collected from edge area. B, Valley splitting energies of X_0 emission as a function of magnetic field, the green data points are collected from the center area and the red data points are collected from the edge area. The nonuniformity of the exfoliated WSe_2, which is visualized by plotting the PL evolution crossing the samples, suggests there is gradually unintentional doping from the center to the edge region. For the valley splitting behavior of X_0 emission, it is almost independent on the doping level. While doping level plays a critical role in the valley splitting behavior of X_T emission

again manifests that the valley splitting behavior of X_0 emission is nearly independent of the doping density.

In the large flake, the valley splitting behavior of the trion emission at the edge region shows a nonlinear dependence with the external magnetic field. While for the smaller flake, it shows a weaken linear dependence with the external magnetic field. This is probably due to the less edge doping effect in the edge region referring to the larger sample. As previously reported in the literature, the smaller flakes have less edge wrinkling compared with the large ones,[40,41] which probably result in the weakening of the physical absorption of O_2 and H_2O. Thus, the edge region of small flake is less easily affected by the O_2 and H_2O in the atmosphere compared with the large one. At the edge of small flake, a small number of holes induced by moisture only facilitate less positive trions. However, at the edge of the large flake, there are more holes accumulated at the edge regions, which results in the formation of more positive intra-valley trions. The different defective sites and/or structures are possibly responsible for the size-dependent valley magnetic response at the edge regions.

To sum up, the valley splitting effects of X_T and X_0 emissions crossing the exfoliated ML WSe_2 flakes are studied by circularly polarized magneto-PL spectroscopy/imaging at a low temperature of 4.2 K. The peak evolutions of X_T and X_0 emissions are due to gradual doping and the edge region is more unintentionally doped due to the lateral contact to the atmosphere during the sample preparation process. In the range of relatively higher doping region, the valley splitting behavior of X_T emission shows the sublinear dependence with the external magnetic field. While in the range of the lower doping region, the valley splitting behavior of X_T emission maintains a linear relationship with the external magnetic field and the slope of the magnetic response decreases with the increasing doping level. The size-dependent physical absorption might be responsible for the variation of the valley splitting behavior of X_T emission. On the other hand, the valley splitting behavior of the X_0 emission is nearly independent of the doping density. This work not only enriches the fundamental study of doping effect on valley splitting but also is beneficial for future valleytronics.

2 | EXPERIMENTAL SECTION

2.1 | Sample preparation

ML WSe_2 flakes were mechanically exfoliated from a purchased bulk WSe_2 crystal (2D semiconductors Inc.) onto a Si substrate capped with the 300 nm SiO_2.

2.2 | Optical measurement

The circularly polarized PL spectra/images were obtained by using a WITec alpha300 Raman/PL system. The samples were placed on a cryogenic stage consisting of *x*-, *y*-, and *z*-axis positioners with an *x*-*y* scanner that can be used for PL mapping up to $30 \times 30\ \mu m^2$. All mapping data were

obtained by using a laser beam of 2.33 eV with a power of ~100 μW.

ACKNOWLEDGMENTS

This work was supported by the National Natural Science Foundation of China (Nos. 61774040 and 11774170), the Shanghai Municipal Science and Technology Commission (No. 18JC1410300), the Fudan University-CIOMP Joint Fund (No. FC2018-002), the National Key R&D Program of China (No. 2018YFA0703700), the National Young 1000 Talent Plan of China, the Shanghai Municipal Natural Science Foundation (No. 16ZR1402500), Singapore Ministry of Education (MOE) Tier 1 RG199/17.

CONFLICT OF INTEREST

The authors declare no conflict of interest.

ORCID

Ting Yu https://orcid.org/0000-0002-0113-2895

REFERENCES

1. Chhowalla M, Shin HS, Eda G, Li LJ, Loh KP, Zhang H. The chemistry of two-dimensional layered transition metal dichalcogenide nanosheets. *Nat Chem*. 2013;5:263-275.
2. Zhang Y, Chang TR, Zhou B, et al. Direct observation of the transition from indirect to direct bandgap in atomically thin epitaxial $MoSe_2$. *Nat Nanotechnol*. 2014;9:111-115.
3. Castro Neto AH, Guinea F, Peres NMR, Novoselov KS, Geim AK. The electronic properties of graphene. *Rev Mod Phys*. 2009;81:109-162.
4. Zeng HL, Cui XD. An optical spectroscopic study on two-dimensional group-VI transition metal dichalcogenides. *Chem Soc Rev*. 2015;44:2629-2642.
5. Zhang F, Kane CL, Mele EJ. Surface states of topological insulators. *Phys Rev B*. 2012;86:081303(R).
6. Yu S, Wu X, Wang Y, Guo X, Tong L. 2D materials for optical modulation: challenges and opportunities. *Adv Mater*. 2017;29:1606128.
7. Duan X, Wang C, Pan A, Yu R, Duan X. Two-dimensional transition metal dichalcogenides as atomically thin semiconductors: opportunities and challenges. *Chem Soc Rev*. 2015;44:8859-8876.
8. Cong C, Shang J, Wang Y, Yu T. Optical properties of 2D semiconductor WS_2. *Adv Opt Mater*. 2018;6:1700767.
9. Shang J, Cong C, Wu L, Huang W, Yu T. Light sources and photodetectors enabled by 2D semiconductors. *Small Methods*. 2018;2:1800019.
10. Mak KF, Shan J. Photonics and optoelectronics of 2D semiconductor transition metal dichalcogenides. *Nat Photonics*. 2016;10:216-226.
11. Choi W, Choudhary N, Han GH, Park J, Akinwande D, Lee YH. Recent development of two-dimensional transition metal dichalcogenides and their applications. *Mater Today*. 2017;20:116-130.
12. Wang QH, Kalantar-Zadeh K, Kis A, Coleman JN, Strano MS. Electronics and optoelectronics of two-dimensional transition metal dichalcogenides. *Nat Nanotechnol*. 2012;7:699-712.
13. Shang J, Cong C, Wang Z, et al. Room-temperature 2D semiconductor activated vertical-cavity surface-emitting lasers. *Nat Commun*. 2017;8:543.
14. Eginligil M, Cao B, Wang Z, et al. Dichroic spin–valley photocurrent in monolayer molybdenum disulphide. *Nat Commun*. 2015;6:7636.
15. Yu H, Cui X, Xu X, Yao W. Valley excitons in two-dimensional semiconductors. *Natl Sci Rev*. 2015;2:57-70.
16. Xu X, Yao W, Xiao D, Heinz TF. Spin and pseudospins in layered transition metal dichalcogenides. *Nat Phys*. 2014;10:343-350.
17. Liu GB, Xiao D, Yao YG, Xu XD, Yao W. Electronic structures and theoretical modelling of two-dimensional group-VIB transition metal dichalcogenides. *Chem Soc Rev*. 2015;44:2643-2663.
18. Sun L, Yan J, Zhan D, et al. Spin-orbit splitting in single-layer MoS_2 revealed by triply resonant Raman scattering. *Phys Rev Lett*. 2013;111:126801.
19. Zeng H, Dai J, Yao W, Xiao D, Cui X. Valley polarization in MoS_2 monolayers by optical pumping. *Nat Nanotechnol*. 2012;7:490-493.
20. Aivazian G, Gong Z, Jones AM, et al. Magnetic control of valley pseudospin in monolayer WSe_2. *Nat Phys*. 2015;11:148-152.
21. Li Y, Ludwig J, Low T, et al. Valley splitting and polarization by the Zeeman effect in monolayer $MoSe_2$. *Phys Rev Lett*. 2014;113:266804.
22. Srivastava A, Sidler M, Allain AV, Lembke DS, Kis A, Imamoğlu A. Valley Zeeman effect in elementary optical excitations of monolayer WSe_2. *Nat Phys*. 2015;11:141-147.
23. MacNeill D, Heikes C, Mak KF, et al. Breaking of valley degeneracy by magnetic field in monolayer $MoSe_2$. *Phys Rev Lett*. 2015;114:037401.
24. Stier AV, McCreary KM, Jonker BT, Kono J, Crooker SA. Exciton diamagnetic shifts and valley Zeeman effects in monolayer WS_2 and MoS_2 to 65 tesla. *Nat Commun*. 2016;7:10643.
25. Plechinger G, Nagler P, Arora A, et al. Excitonic valley effects in monolayer WS_2 under high magnetic fields. *Nano Lett*. 2016;16:7899-7904.
26. Wang Z, Mak KF, Shan J. Strongly interaction-enhanced valley magnetic response in monolayer WSe_2. *Phys Rev Lett*. 2018;120:066402.
27. Jones AM, Yu H, Ghimire NJ, et al. Optical generation of excitonic valley coherence in monolayer WSe_2. *Nat Nanotechnol*. 2013;8:634-638.
28. Li H, Lu G, Wang Y, et al. Mechanical exfoliation and characterization of single- and few-layer nanosheets of WSe_2, TaS_2, and $TaSe_2$. *Small*. 2013;9:1974-1981.
29. Sahin H, Tongay S, Horzum S, et al. Anomalous Raman spectra and thickness-dependent electronic properties of WSe_2. *Phys Rev B*. 2013;87:165409.
30. Srivastava A, Sidler M, Allain AV, Lembke DS, Kis A, Imamoglu A. Optically active quantum dots in monolayer WSe_2. *Nat Nanotechnol*. 2015;10:491-496.

31. You Y, Zhang X, Berkelbach TC, Hybertsen MS, Reichman DR, Heinz TF. Observation of biexcitons in monolayer WSe_2. *Nat Phys*. 2015;11:477-481.
32. Shang J, Cong C, Shen X, et al. Revealing electronic nature of broad bound exciton bands in two-dimensional semiconducting WS_2 and MoS_2. *Phys Rev Mater*. 2017;1:074001.
33. Teke A, Özgür Ü, Doğan S, et al. Excitonic fine structure and recombination dynamics in single-crystalline ZnO. *Phys Rev B*. 2004;70:195207.
34. Tongay S, Zhou J, Ataca C, et al. Broad-range modulation of light emission in two-dimensional semiconductors by molecular physisorption gating. *Nano Lett*. 2013;13:2831-2836.
35. Ugeda MM, Bradley AJ, Shi SF, et al. Giant bandgap renormalization and excitonic effects in a monolayer transition metal dichalcogenide semiconductor. *Nat Mater*. 2014;13:1091-1095.
36. Portella-Oberli MT, Ciulin V, Berney JH, Deveaud B, Kutrowski M, Wojtowicz T. Interacting many-body systems in quantum wells: evidence for exciton-Trion-electron correlations. *Phys Rev B*. 2004;69:235311.
37. Schmitt-Rink S, Chemla DS, Miller DAB. Theory of transient excitonic optical nonlinearities in semiconductor quantum-well structures. *Phys Rev B*. 1985;32:6601-6609.
38. Gao S, Liang Y, Spataru CD, Yang L. Dynamical excitonic effects in doped two-dimensional semiconductors. *Nano Lett*. 2016;16:5568-5573.
39. Wang G, Bouet L, Glazov MM, et al. Magneto-optics in transition metal diselenide monolayers. *2D Mater*. 2015;2:034002.
40. Zheng Q, Geng Y, Wang S, Li Z, Kim J-K. Effects of functional groups on the mechanical and wrinkling properties of graphene sheets. *Carbon*. 2010;48:4315-4322.
41. Luxa J, Jankovský O, Sedmidubský D, et al. Origin of exotic ferromagnetic behavior in exfoliated layered transition metal dichalcogenides MoS_2 and WS_2. *Nanoscale*. 2016;8:1960-1967.

SUPPORTING INFORMATION

Additional supporting information may be found online in the Supporting Information section at the end of this article.

How to cite this article: Zou C, Zhang H, Chen Y, et al. Spatial variations of valley splitting in monolayer transition metal dichalcogenide. *InfoMat*. 2020;2:585–592. https://doi.org/10.1002/inf2.12050